Available online at www.sciencedirect.com
ScienceDirect
Energy 32 (2007) 406–417
ENERGY
www.elsevier.com/locate/energy

Modeling and control of a SOFC-GT-based autonomous power system

Rambabu Kandepu[a,*], Lars Imsland[b], Bjarne A. Foss[a], Christoph Stiller[c], Bjørn Thorud[c], Olav Bolland[c]

[a]*Department of Engineering Cybernetics, Norwegian University of Science and Technology, Trondheim, 7491, Norway*
[b]*SINTEF ICT, 7465 Trondheim, Norway*
[c]*Department of Energy and Process Engineering, Norwegian University of Science and Technology, Trondheim, 7491, Norway*

Received 31 October 2005

Abstract

In this article, a dynamic, lumped model of a solid oxide fuel cell (SOFC) is described, as a step towards developing control relevant models for a SOFC combined with a gas turbine (GT) in an autonomous power system. The model is evaluated against a distributed dynamic tubular SOFC model. The simulation results confirm that the simple model is able to capture the important dynamics of the SOFC and hence it is concluded that the simple model can be used for control and operability studies of the hybrid system. Several such lumped models can be aggregated to approximate the distributed nature of important variables of the SOFC. Further, models of all other components of a SOFC-GT-based autonomous power system are developed and a control structure for the total system is developed. The controller provides satisfactory performance for load changes at the cost of efficiency.

Keywords: SOFC; Control relevant modeling; Hybrid system; Control

1. Introduction

In the foreseeable future, fossil fuels including natural gas will be a major source of energy. With today's increasing concern about global warming and climate change, there is an incentive to investigate natural gas power processes that operate efficiently, thus emitting less per kWh produced, and also power production processes with CO_2 capture capabilities. It is widely accepted that fuel cells are power sources that will become increasingly important, due to high efficiency, low levels of pollution and noise, and high reliability. One of the most promising fuel cell technologies is the solid oxide fuel cell (SOFC), due to its solid state design and internal reforming of gaseous fuels, in addition to its high efficiency [1]. The SOFC converts the chemical energy of a fuel directly to electrical energy. The electrical efficiency of a SOFC can reach 55%. Another significant advantage of the SOFC is that since it operates at high temperature and its efficiency increases when pressurized, it naturally lends itself as a heat source for a gas turbine (GT) cycle. The combined (hybrid) cycle can theoretically have an overall electrical efficiency of up to 70% with a power range from a few hundred kWs to a few MWs [1]. Processes based on SOFCs can be used as power processes with CO_2 capture, since the "used fuel" (including water and CO_2) and air exit streams can be kept separated [2]. The main applications of the hybrid system include remote area power supply and distributed power generation.

There are several models available in the literature for SOFC-GT hybrid systems [3–6]. In [7], a dynamic model of a grid-connected SOFC model is developed. However, to the best of authors' knowledge there is no model in the literature with integration of a SOFC-GT hybrid system with a power grid and an electrical load. The reason for developing such an integrated model is to obtain a comprehensive understanding of the operability of the system which has close dynamic interactions between the power generation system and the local grid. Further, the hybrid system consists of tightly integrated dynamic subsystems with strict operating criteria making the control

*Corresponding author. Tel.: +47 73594482; fax: +47 73594399.
E-mail address: Rambabu.Kandepu@itk.ntnu.no (R. Kandepu).

0360-5442/$ - see front matter © 2006 Elsevier Ltd. All rights reserved.
doi:10.1016/j.energy.2006.07.034

design more challenging in terms of disturbance rejection, part-load operation and in particular start-up, shutdown and load shedding. Suitable system actuation must be chosen, good control structures must be devised, and good controllers must be designed. As a basis for all these tasks, control relevant models must be developed for the subsystems, and for the total system. Such models should have limited complexity to allow for the necessary analysis, while at the same time should include the important dynamic interactions.

In this paper we present an integrated model of a SOFC-GT hybrid system with a power grid connecting to an electrical load. A control relevant model of the SOFC is developed with no geometric regard and it is evaluated with a detailed model. Further models of all other components of the power system are described including the main underlying assumptions. The system model is subsequently used to perform analysis of system dynamics. A simple control design is proposed and assessed through a set of simulation scenarios.

2. Process description

A schematic diagram of the integrated system where the SOFC-GT hybrid system is connected to the load by a bus bar is shown in Fig. 1. Methane (fuel) is mixed with a part of the anode flue gas and is partially steam reformed in a pre-reformer generating hydrogen. The heat required for endothermic reformation reactions in the pre-reformer is supplied from the SOFC stack through radiation. The gas mixture from the pre-reformer is fed to the anode volume of the SOFC, where the remaining part of the methane is reformed. Compressed atmospheric air is heated in a recuperative heat exchanger and is used as an oxygen source at the cathode side of the SOFC. In the SOFC, electrochemical reactions take place and DC electric power is produced. The rate of the electrochemical reactions depends on the current. A part of the anode flue gas is recycled to supply steam to the pre-reformer. The remaining part of the anode and cathode flue gases is supplied to a combustion chamber where the unused fuel is combusted. In a CO_2 capture setting, mixing of the anode and cathode flue gases should be avoided, but this is not treated herein.

The hybrid system is modeled using both single-shaft and double-shaft configurations. We will however focus on the double-shaft configuration in the simulations as in Fig. 1. The combusted gas mixture is expanded in a high-pressure turbine (HPT) with variable shaft speed driving the compressor. The HPT flue gas is further expanded to atmospheric pressure in a low-pressure turbine (LPT) with constant shaft speed, which is coupled to a synchronous generator producing AC electric power. The expanded gas mixture is used to heat up the compressed air in a heat exchanger. The DC power from the SOFC stack is fed to an inverter which converts DC to AC with a fixed frequency. The inverter and the generator are connected to a local grid, which is connected to a electric load. Both the SOFC stack and the generator supply the electric load demand on the grid. The load sharing between the SOFC stack and the generator cannot be controlled when there is a load change on the grid, even though the load sharing between the SOFC stack and the generator will change. Typically 60%–70% of the total power is supplied by the SOFC stack.

3. SOFC modeling

3.1. SOFC process description

The SOFC is a device which converts chemical energy of a fuel directly into electrical energy [1]. The basic

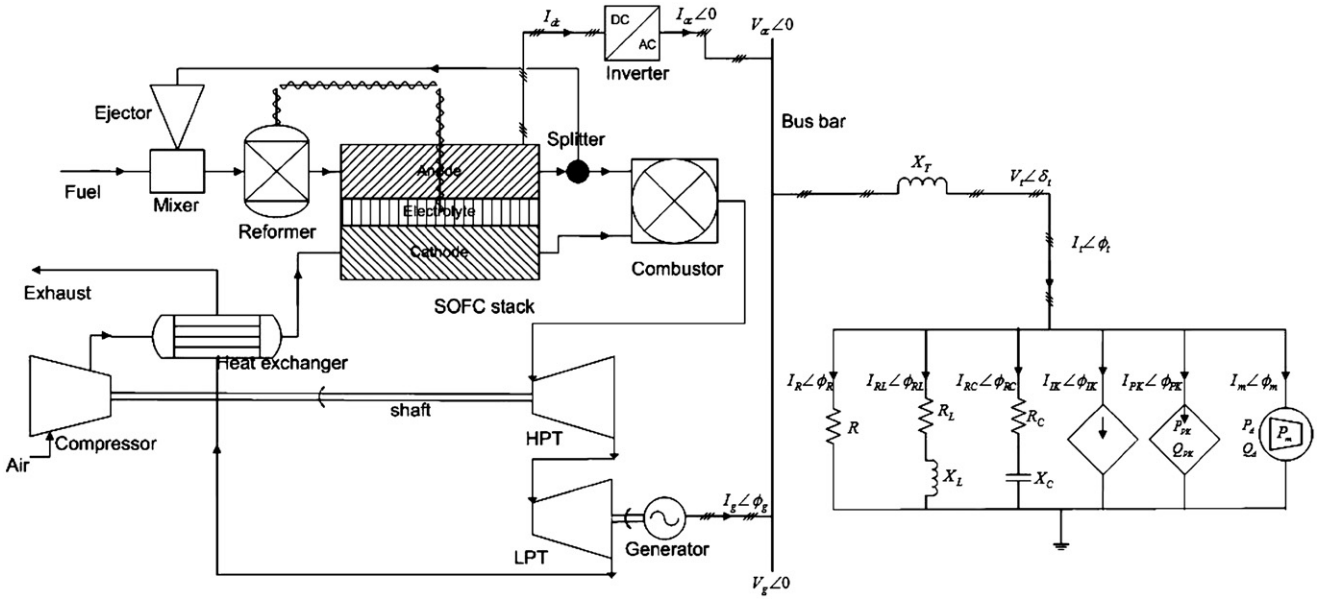

Fig. 1. SOFC-GT hybrid system integrated with autonomous power system.

components of the SOFC are anode, cathode and electrolyte as conceptually illustrated in Fig. 2. Fuel is supplied to the anode and air is supplied to the cathode. At the cathode–electrolyte interface, oxygen molecules accept electrons coming from the external circuit to form oxide ions, see Table 1 for reactions. The electrolyte layer allows only oxide ions to pass through and at the anode–electrolyte interface, hydrogen molecules present in the fuel react with oxide ions to form steam, and electrons get released. These electrons pass through the external circuit and reach the cathode–electrolyte layer, and thus the circuit is closed. To increase the amount of power generated, a number of cells can be connected in series/parallel. This is known as stacking of cells. Also, there are mainly two types of SOFCs depending on the cell geometry; tubular and planar. The operating pressure can be from 1 to 15 bar. It is found that SOFCs show enhanced performance with increasing cell pressure [1]. The operating temperature of the SOFC is around 800–1000°C. The high temperature and pressure operating conditions of the SOFC make it advantageous to combine the SOFC with a GT to get a hybrid system with an high efficiency [5]. Due to the high operating temperature, several types of fuels can be used. In this paper methane is used as fuel. Because of the electrochemical reactions, there is a production of steam, and partial recirculation of this steam is used to reform methane into hydrogen. Typically, one third of the fuel is reformed, for example in a pre-reformer, before it enters the SOFC and the remaining part is reformed within

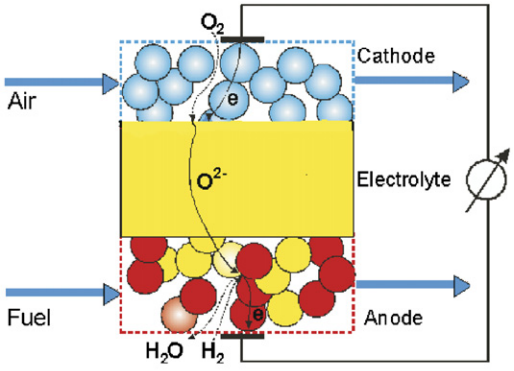

Fig. 2. SOFC operation.

Table 1
Reactions at anode and cathode

Anode reaction	Reaction rate (r_j^{an})
$H_2 + O^{2-} \rightarrow H_2O + 2e^-$	r_1^{an}
$CH_4 + H_2O \Leftrightarrow CO + 3H_2$	r_2^{an}
$CO + H_2O \Leftrightarrow CO_2 + H_2$	r_3^{an}
$CH_4 + 2H_2O \Leftrightarrow CO_2 + 4H_2$	r_4^{an}
Cathode reaction	
$\frac{1}{2}O_2 + 2e^- \rightarrow O^{2-}$	r_1^{ca}

Table 2
Notation for components

i	1	2	3	4	5	6	7
Components	N_2	O_2	H_2	CH_4	H_2O	CO	CO_2

the SOFC. Table 1 gives the list of reactions that take place at anode and cathode and the corresponding reaction rates notation.

The dynamic model of a single SOFC is developed using two mass balances; one for anode volume and the other for cathode volume, and one overall energy balance. In all of the streams from/to the SOFC, the following components can be present: nitrogen (N_2), oxygen (O_2), Hydrogen (H_2), methane (CH_4), steam (H_2O), carbonmonoxide (CO), and carbondioxide (CO_2). A number, as shown in Table 2, is assigned to each of these components to simplify the notation.

3.2. Model assumptions

The following main assumptions are made in developing the model:

(1) All the physical variables are assumed to be uniform over one SOFC, resulting in a lumped cell model.
(2) There is sufficient turbulence and diffusion within the anode and the cathode for perfect mixing to occur (CSTR).
(3) The gas temperatures within the SOFC are assumed to be the same as the solid; i.e. the thermal inertia of the gases is neglected.
(4) For the energy balance, pressure changes within the SOFC are neglected.
(5) All gases are assumed to be ideal.
(6) All cells in the stack are assumed to operate identically.

3.3. Mass balance

Two mass balances; one for the anode volume and one for the cathode volume are used:

$$\frac{dN_i^{an}}{dt} = \dot{N}_i^{in,an} - \dot{N}_i^{out,an} + \sum_{j=1}^{n_{rx}^{an}} a_{ij}^{an} r_j^{an},$$

$$i = 1, \ldots, 7, \quad n_{rx}^{an} = 4,$$

$$\frac{dN_i^{ca}}{dt} = \dot{N}_i^{in,ca} - \dot{N}_i^{out,ca} + \sum_{j=1}^{n_{rx}^{ca}} a_{ij}^{ca} r_j^{ca},$$

$$i = 1, \ldots, 7, \quad n_{rx}^{ca} = 1.$$

The reaction rates corresponding to the electrochemical reactions (r_1^{ca}, r_1^{an}) are directly related by the current,

$$r_1^{an} = I/(2F) = r_1^{ca} \tag{1}$$

and the reaction rates corresponding to the reforming reactions are calculated as proposed by Xu [8]

$$r_2^{an} = \frac{k_2}{p_{H_2}^{an^2.5}}\left(p_{CH_4}^{an}p_{H_2O}^{an} - \frac{p_{H_2}^{an^3}p_{CO}^{an}}{K_2}\right)\Big/(DEN)^2,$$

$$r_3^{an} = \frac{k_3}{p_{H_2}^{an}}\left(p_{CO}^{an}p_{H_2O}^{an} - \frac{p_{H_2}^{an}p_{CO_2}^{an}}{K_3}\right)\Big/(DEN)^2,$$

$$r_4^{an} = \frac{k_4}{p_{H_2}^{an^{3.5}}}\left(p_{CH_4}^{an}p_{H_2O}^{an^2} - \frac{p_{H_2}^{an^4}p_{CO_2}^{an}}{K_4}\right)\Big/(DEN)^2. \quad (2)$$

In (2), DEN is given by

$$DEN = 1 + K_{CO}^{ads}p_{CO}^{an} + K_{H_2}^{ads}p_{H_2}^{an} + K_{CH_4}^{ads}p_{CH_4}^{an} + K_{H_2O}^{ads}p_{H_2O}^{an}/p_{H_2}^{an} \quad (3)$$

and k_2, k_3 and k_4, the rate coefficients for the reforming reactions, are calculated by

$$k_j = A_{kj}\exp\left(\frac{-E_j}{RT}\right), \quad j = 2,3,4. \quad (4)$$

The equilibrium constants for the reforming reactions K_2, K_3 and K_4 are given by

$$K_2 = \exp(-26830/T + 30.114)[\text{bar}^2],$$

$$K_3 = \exp(4400/T - 4.036)[-],$$

$$K_4 = \exp(-22430/T + 26.078)[\text{bar}^2]. \quad (5)$$

In (3), $K_{CO}^{ads}, K_{H_2}^{ads}, K_{CH_4}^{ads}$ and $K_{H_2O}^{ads}$ are the adsorption constants, which are calculated by

$$K_i^{ads} = A_{K^{ads}i}\exp\left(\frac{-\Delta\overline{h}_i^{ads}}{RT}\right), \quad i = H_2, CH_4, H_2O, CO. \quad (6)$$

It is assumed that the exhaust flows at the anode and cathode outlets can be described by the choked exhaust flow equation. This means that the mass flow rate of the exhaust flow at the anode (cathode) depends on the pressure difference between the pressure inside the anode (cathode) and the pressure at the outlet [23]:

$$\dot{m}_{out,an} = \sqrt{k_{an}(p_{an} - p_{out,an})},$$

$$\dot{m}_{out,ca} = \sqrt{k_{ca}(p_{ca} - p_{out,ca})}. \quad (7)$$

The partial pressures, volume, and temperature are assumed to be related by the ideal gas equation, for instance at the anode,

$$p_i^{an}V_{an} = N_i^{an}RT. \quad (8)$$

3.4. Energy balance

The energy balance accounts for the whole SOFC volume, and is given by [9,10]

$$C^s\frac{dT}{dt} = \sum_{i=1}^{N}\dot{N}_i^{in,an}(\Delta\overline{h}_i^{in,an} - \Delta\overline{h}_i) + \sum_{i=1}^{N}(\dot{N}_i^{in,ca}(\Delta\overline{h}_i^{in,ca} - \Delta\overline{h}_i) - \sum_{j=1}^{M}\Delta\overline{h}_j^{rx}r_j^{an} - P_{DC} - P_{rad} - P_{cond}. \quad (9)$$

In this equation, the dynamics of the temperature changes of gases are neglected as they are fast compared to the temperature changes of the solid. Hence the energy balance gives a dynamic equation for the temperature changes of the SOFC solid.

In (9), P_{DC} represents the amount of DC power produced by the SOFC, P_{cond} represents the conduction heat loss from SOFC to the surroundings and P_{rad} represents the amount of radiation heat given from the SOFC. As the SOFC operating temperature is higher than that of the surroundings, there is always some loss due to radiation. It can be calculated by [11]

$$P_{rad} = A\delta\varepsilon\sigma(T^4 - T_{sur}^4). \quad (10)$$

In (10), A is the surface area, δ is shaping factor, T_{sur} represents the surroundings temperature, ε is the emissivity of the SOFC surface and σ is the *Stefan–Boltzmann constant* ($\sigma = 5.67 \times 10^{-8}\,\text{W}/(\text{m}^2\,\text{K}^4)$).

The amount of DC power from the SOFC is given by

$$P_{DC} = VI. \quad (11)$$

Moreover, air utilization (AU) and fuel utilization (FU) are defined as

$$\text{AU} = 1 - \frac{\dot{N}_{O_2}^{out}}{\dot{N}_{O_2}^{in}}, \quad \text{FU} = 1 - \frac{\dot{N}_{H_2}^{out}}{\dot{N}_{H_2}^{in}}. \quad (12)$$

The AU and FU are included in the model as they are identified as important variables in representing the SOFC state [6]. Recycle ratio is defined as the ratio of the fuel flow recycled to the fuel flow at the anode outlet.

3.5. Voltage

The operating cell voltage is given by

$$V = E^{OCV} - V_{loss}, \quad (13)$$

where the open circuit voltage of the cell is given by the *Nernst equation* [1],

$$E^{OCV} = E^o + \frac{RT}{2F}\ln\left(\frac{p_{H_2}^{an}p_{O_2}^{an^{0.5}}}{p_{H_2O}^{an}}\right), \quad (14)$$

where E^o is the EMF at standard pressure. V_{loss} is the voltage loss. Stiller et al. [12], Thorud et al. [6], Campanari et al. [13], and Magistri et al. [3] used rather complex empirical functions to calculate the voltage loss. In this simple model the voltage loss is approximated by a first

order function of cell temperature and current. This function is obtained by curve fitting the simulated data obtained from a distributed model [6]. Thus, total voltage loss is calculated by

$$V_{loss} = C_1 I + C_2 T + C_3, \tag{15}$$

where C_1, C_2 and C_3 are constants.

3.6. Model aggregation

In a real SOFC, temperature and pressure vary over the SOFC volume. The distributed nature cannot be represented by using the "one volume" model. By connecting many volumes in a sequential manner it is possible to approximate the distributed nature of the variables. The whole structure with all the volumes represent a single cell. So, if many volumes are connected, each volume can be represented by a scaled-down model. In principle, it is possible to connect any number of volumes, but for simplification, an example is considered where a single SOFC model is obtained by connecting two scaled-down models as shown in Fig. 3. The two volumes are selected such that the first volume is represented by a scaled-down model by scaling down the "one volume" model volume and heat capacity constants by α where $0<\alpha<1$ and typically $\alpha = \frac{1}{3}$. The second volume is represented by a scaled-down model obtained by scaling down the "one volume" model constants by $1-\alpha$. Electrically, the two scaled-down models are connected in parallel (Fig. 4). Ideally, the voltage across each of the volumes should be the same and the total current is divided between the two volumes. Then most of the current is produced from the second volume, as mainly reforming reactions take place in the first volume. In the present work it is assumed that the first volume supplies 1/3rd of the total current and the second volume supplies the remaining current. With this assumption, there is a small voltage difference between the two volumes. Developing a strategy for dividing the currents among the volumes when a SOFC is represented by many volumes is a part of further work. The basic point is to show that it is possible to approximate the distributed nature of the variables by aggregating the scaled-down models.

4. Power system modeling

4.1. Reformer

A reformer is used to convert methane into hydrogen by steam reforming. It is a fixed volume reactor having two inlets, one for methane and the other for steam and one outlet. The assumptions made in the model development of the reformer are the same as those of the SOFC. The dynamic model is developed using one mass balance and one energy balance. The three reformation reactions considered are given in Table 1. The reformation is a highly endothermic process, so heat must be supplied to the reactor. As the SOFC operates at a high temperature, there is radiation from the SOFC stack and this can be supplied to the reformer by using a suitable mechanical design. The operating temperature of the reactor is in the range 500–700 °C.

4.2. Heat exchanger

A very simple model of a counter-flow heat exchanger is used, in which the amount of the heat exchanged depends on the heat transfer coefficient of the exchanger wall and also on the average temperature difference between the hot and cold streams. A first order transfer function describes the dynamics of the temperatures of both the streams. The following assumptions were made:

(1) The model is lumped. All the physical parameters are assumed to be uniform over the heat exchanger.
(2) There is no pressure loss within the heat exchanger.

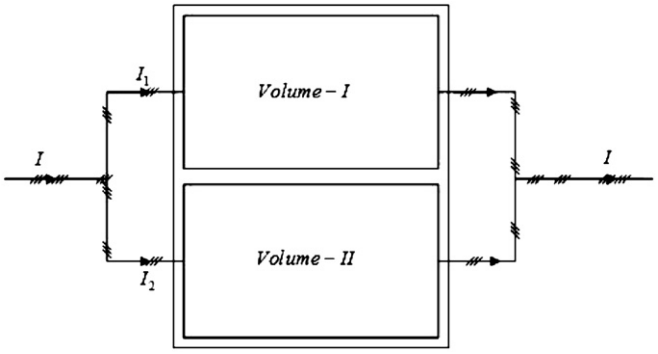

Fig. 4. Electrical aggregation.

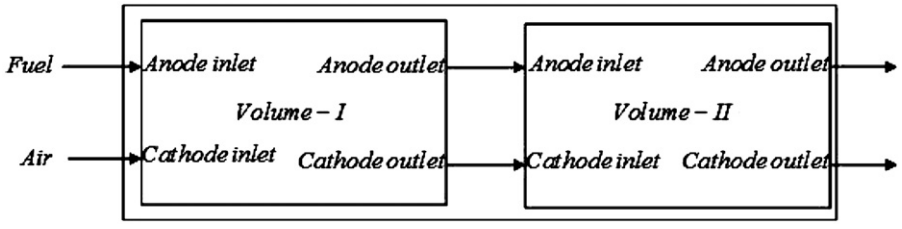

Fig. 3. Aggregation mechanically.

4.3. Combustion chamber

The combustion chamber as shown in Fig. 1, has 2 inlet streams and one outlet stream. It burns the fuel coming from all the inlet flows in the presence of air. The operating conditions will always be such that there is surplus oxygen available for complete combustion due to the fact that air mass flow rate is much larger than the fuel mass flow rate. In this model, the fuel can be methane, hydrogen or carbonmonoxide or a mixture of these fuels. The following reactions are being considered during the combustion:

$$2H_2 + O_2 \rightarrow 2H_2O,$$

$$CH_4 + 2O_2 \rightarrow 2H_2O + CO_2,$$

$$2CO + O_2 \rightarrow 2CO_2. \tag{16}$$

The following assumptions are made:

(1) The pressures of all the inlet flows are the same.
(2) As the combustion process is very rapid, it is modeled as an instantaneous process and complete combustion is assumed.
(3) The model is a bulk model, i.e. all physical variables are assumed to be uniform over the combustion chamber.
(4) There is a 2% pressure loss in the combustor volume.

The following mass and energy balances are used for the control volume:

$$\sum_{k=1}^{n_{in}} \dot{N}_i^{in,k} + \sum_{j=1}^{n_{rx}} a_{ij} r_j = \dot{N}_i^{out}, \quad i = 1, \ldots, 7,\ n_{rx} = 3,$$

$$\sum_{k=1}^{n_{in}} \sum_{i=1}^{N} (\dot{N}_i^{in,k} \Delta\overline{h}_i^{in,k} - \sum_{i=1}^{N} \dot{N}_i^{in,k} \Delta\overline{h}_i) - \sum_{j=1}^{M_c} \Delta\overline{h}_j^{rx} r_j = 0,$$

where $N = 7$ is the number of components, $M_c = 3$ is the number of reactions as given in (16) and n_{in} is the number of inlet streams. Otherwise, the notation is similar to (9).

4.4. GT

Compressor and turbine models are based on steady-state performance map characteristics [14]. The map is modeled using polynomials of fourth and fifth order for reduced mass flow, pressure and efficiency as functions of reduced shaft speed and operation line. The following are the assumptions made in both the compressor and turbine models:

(1) The process has constant isentropic efficiency.
(2) The working fluid satisfies the ideal gas equation.

A shaft model accounts for the dynamics of the rotating mass in the GT system which is modeled as

$$\dot{\omega} = P_b/(I\omega), \tag{17}$$

where P_b is the power balance across the shaft, I is the moment of inertia of the rotating mass and, ω is the angular velocity of the shaft.

4.5. Inverter

A simple model of an inverter is developed with the following assumptions:

(1) Power loss is negligible.
(2) Pulse width modulation (PWM) technique is used to control the AC output voltage and frequency. The controller dynamics are neglected as they are fast compared to the hybrid system dynamics.
(3) The inverter supplies AC power at unity power factor.

The power balance on both sides is given by

$$P_{dc} = V_{ac} I_{ac}. \tag{18}$$

4.6. Synchronous generator

The per-phase equivalent circuit of the synchronous generator is shown in Fig. 5 taken from [15]. The magnitude of the electro-motive force (EMF) induced in each phase is assumed to be directly proportional to the shaft speed (ω_g) and field current (I_{fg}),

$$E_g = k_g I_{fg} \omega_g, \tag{19}$$

where k_g is the proportionality constant. The open circuit voltage $V_g\angle 0$, which is taken as the reference in phasor notation, and $E_g\angle\delta_g$ are related as

$$E_g\angle\delta_g = V_g\angle 0 + X_g\angle 90^\circ I_g\angle\phi_g, \tag{20}$$

where $I_g\angle\phi_g$ is the generator current, X_g is the stator per-phase reactance in ohms. It is assumed that there is a 2% power loss in conversion from mechanical to electrical energy which includes rotational loss, copper loss and magnetizing loss. The generator is connected to a power turbine which runs at a constant speed. Hence, the frequency of the AC supply from the generator is assumed constant. The real and reactive powers supplied by the generator are given by

$$P_g = V_g I_g \cos\phi_g,$$

$$Q_g = V_g I_g \sin\phi_g. \tag{21}$$

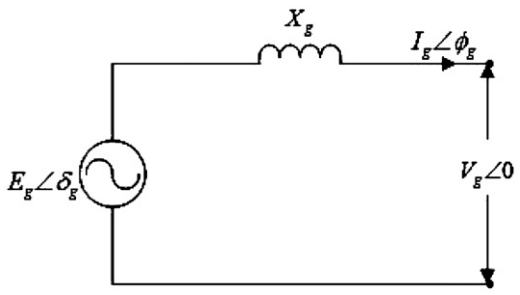

Fig. 5. Per-phase equivalent circuit of synchronous generator.

4.7. Autonomous power grid

The integrated SOFC-GT hybrid system with the autonomous power grid is shown in Fig. 1 [7]. The model of the grid and load is chosen such that the level of complexity is comparable to the SOFC-GT hybrid system models. The bus bar voltage is fixed at 230 V and is taken as the reference in phasor notation. We assume that the generator field current is controlled such that the generator terminal voltage $V_g\angle 0$ is equal to the bus bar voltage $V_{ac}\angle 0$. The bus bar is connected to the load by transmission lines of reactance X_T. The load is represented by six parallel branches with different components in each branch as shown in Fig. 1. It is categorized into four types of loads; constant impedance, constant current, constant power and induction motor load. The constant impedance, constant current and constant power load represent the residential loads such as lights, water heaters, ovens etc. The induction motor load is considered to represent an industrial load [16]. The constant impedance load is represented by the first three branches with resistive, inductive and capacitive loads. The fourth and fifth branches represent the constant current and constant power loads, respectively. The sixth branch represents the induction motor load. The total load current $I_t\angle\phi_t$ is the sum of the currents from the inverter and the synchronous generator,

$$I_t\angle\phi_t = I_{ac}\angle 0 + I_g\angle\phi_g. \tag{22}$$

As it is assumed that the inverter supplies power at unity power factor, the generator supplies the load and transmission line reactive power. The load voltage $V_t\angle\delta_t$ is given by

$$V_t\angle\delta_t = V_{ac}\angle 0 - X_T\angle 90^\circ I_t\angle\phi_t. \tag{23}$$

The first three branches of the load (R, RL, RC branches) are used to model different constant impedance loads. The currents in these branches are given by

$$V_t\angle\delta_t = RI_R\angle\phi_R,$$

$$V_t\angle\delta_t = (R_L + X_L\angle 90^\circ)I_{RL}\angle\phi_{RL},$$

$$V_t\angle\delta_t = (R_C - X_C\angle 90^\circ)I_{RC}\angle\phi_{RC}. \tag{24}$$

The fourth branch is used to model constant current loads where the current $I_{IK}\angle\phi_{IK}$ is assigned a constant value. The fifth branch is used to model constant power loads where real and reactive powers (P_{PK}, Q_{PK}) are assigned constant values and the current $I_{PK}\angle\phi_{PK}$ is calculated by

$$P_{PK} = V_t I_{PK}\cos(\phi_{PK} - \delta_t),$$

$$Q_{PK} = V_t I_{PK}\sin(\phi_{PK} - \delta_t). \tag{25}$$

The last branch is used to model induction motor, whose equivalent circuit is shown in Fig. 6 [17]. Assuming the magnetizing inductance is large, i.e. $X_M \to \infty$, the magnetizing current $I_M\angle\phi_M$ is neglected [17]. The induction motor model equations are then given by

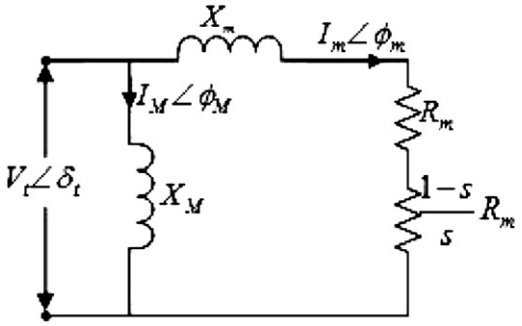

Fig. 6. Equivalent circuit of induction motor.

$$\frac{ds}{dt} = \frac{1}{I\omega_o^2}\left(\frac{P_m}{1-s} - P_d\right),$$

$$V_t\angle\delta_t = \left(\frac{R_m}{s} + X_m\angle 90^\circ\right)I_m\angle\phi_m,$$

$$P_d = V_t I_m\cos(\phi_m - \delta_t),$$

$$Q_d = V_t I_m\sin(\phi_m - \delta_t), \tag{26}$$

where I is moment of inertia of induction motor, ω_o is stator frequency, P_m is mechanical load power on the induction motor, P_d and Q_d are real and reactive power from induction motor, and s is slip given by $s = (\omega_o - \omega_m)/\omega_m$, where ω_m is induction motor speed.

All the components of the hybrid system and the autonomous power system are modeled in the modular modeling environment gPROMS [18].

5. SOFC model evaluation

As no experimental data is available to the authors for evaluating the simple model, the model is evaluated with an available detailed model. The detailed model [6,14,19,20] is a quasi two-dimensional dynamic model of a SOFC tube, similar to that of Siemens Westinghouse. It is a discretized model where gas flows are treated as one-dimensional plug flows. The solid structures are modeled by a two-dimensional discretization scheme in the axial and radial direction, neglecting effects in the circumferential direction. Both the simple and the detailed models are developed using gPROMS [18]. The detailed model includes about 1300 differential equations, whereas the simple model has 15 differential equations.

To evaluate the SOFC model a part of the system shown in Fig. 1, as shown in Fig. 7 is simulated. The results are compared to the detailed model in [6]. The simulations are performed in such a way that the same input conditions are applied to the two SOFC models. The values of some key parameters of the simple model are given in Table 3 while the values of some important variables at steady state are given in Table 4. Table 5 shows the simulation scenarios

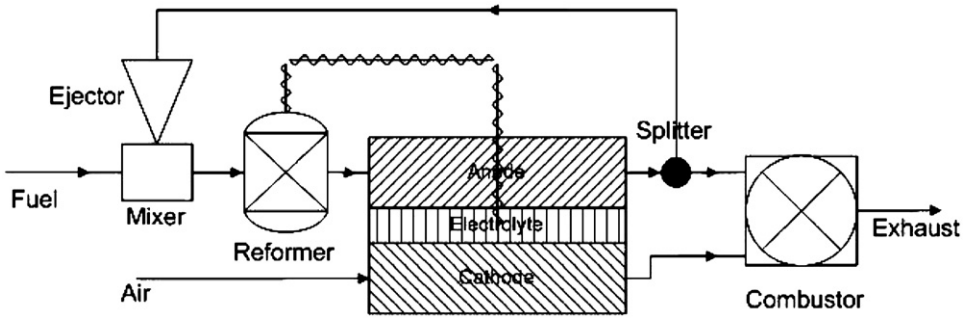

Fig. 7. SOFC system.

Table 3
Model parameters

Anode volume	$1.032 \times 10^{-5}\,m^3$
Cathode volume	$4.3 \times 10^{-5}\,m^3$
C^s	800 J/K
k_{an}	$1.9 \times 10^{-3}\,kg^2\,s^{-2}\,Pa^{-1}$
k_{ca}	$4.2 \times 10^{-3}\,kg^2\,s^{-2}\,Pa^{-1}$

Table 4
Steady state values

Methane flow rate	4.50×10^{-4} kg/s
Methane inlet temperature	950 K
Air flow rate	1.44×10^{-2} kg/s
Air inlet temperature	950 K
Current	250 A
Anode pressure	3 bar
Cathode pressure	3 bar
Cell voltage	0.56 V
Cell power	141 W
Cell temperature	1113 K
Air utilization	0.21
Fuel utilization	0.7

Table 5
Simulation details

Time (min)	Disturbance
90	Fuel flow is decreased by 20%
180	Fuel flow is increased back to 100%
270	Air flow is decreased by 20%
360	Air flow is increased back to 100%
450	Current is decreased by 20%
540	Current is increased back to 100%

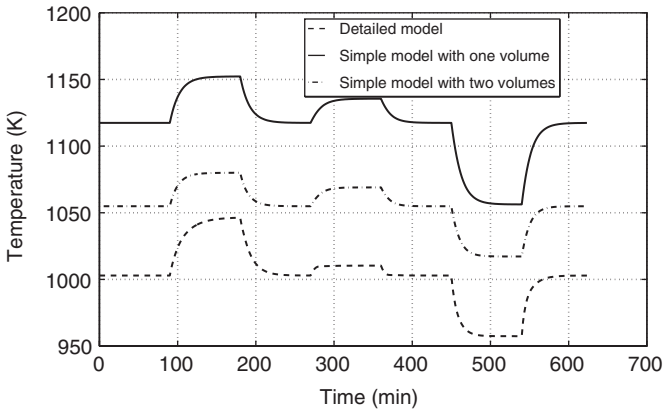

Fig. 8. Comparison of mean solid temperatures of the simple model with one volume and the detailed model for different disturbances.

used for comparing the dynamic behavior of the two models.

Simulations are made for two comparison schemes; first, the simple SOFC model with one volume is compared to the distributed tubular SOFC model [6], and second, the simple SOFC with two volumes is compared to the distributed tubular SOFC model. SOFC mean solid temperature, cell voltage and cell power of the simple model and the detailed model are compared in each comparison scheme. Figs. 8–10 show simulation results from the two comparison schemes.

5.1. Discussion

5.1.1. One volume SOFC model

Fig. 8 shows the mean temperatures of the simple and the detailed SOFC models. At nominal steady state there is a temperature difference of about 120 K between the two mean SOFC temperatures. This can be explained as follows. For both SOFC models, since inlet massflows and current are the same, the energy balance should ensure that the energy in the outlet massflow (and hence outlet temperature) is approximately[1] the same for both models. In a SOFC, the maximum temperature region is at the outlets of the anode and the cathode. Since the simple model is a bulk model, the exit temperature is equal to the mean temperature. For the detailed model, SOFC temperature is a distributed variable and the mean temperature is certainly less than the exit temperature. It is verified that the maximum temperature of the detailed model at the nominal steady state is approximately equal to the mean temperature of the simple SOFC model. From Fig. 8, it is clear that both the models exhibit similar dynamics for the

[1]A slight difference in voltage and hence produced DC power gives a small temperature difference.

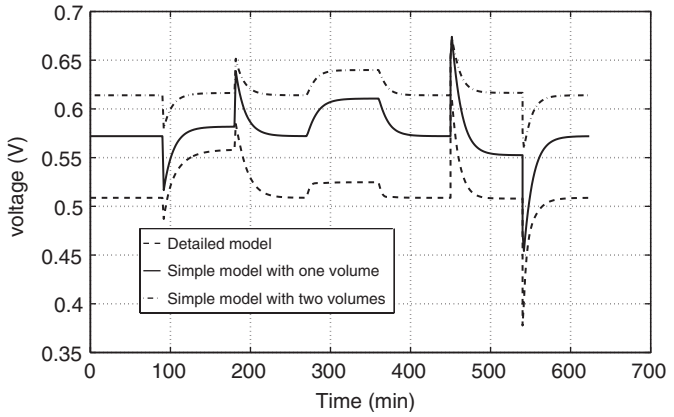

Fig. 9. Comparison of voltages of the simple model with one volume and the detailed model for different disturbances.

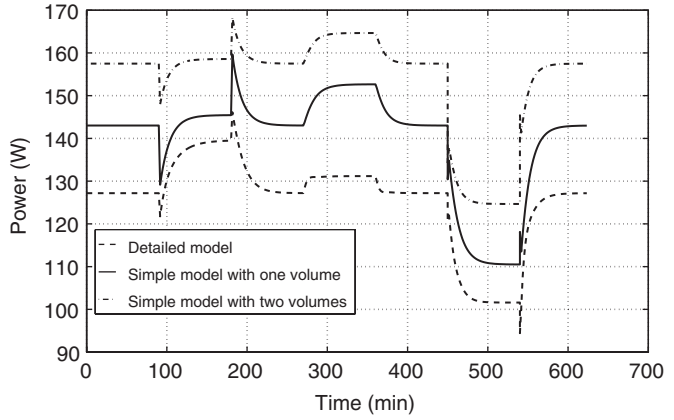

Fig. 10. Comparison of power production of the simple model with one volume and the detailed model for different disturbances.

disturbances applied during the simulation. Fig. 9 shows the voltages of the two models during the simulation. Here also both models show the same dynamic changes in the voltages for all the disturbances applied. Here the simple model has higher voltage than the detailed model which is also mainly because of the higher mean solid temperature of the simple SOFC model. Referring to (15), when temperature increases the voltage loss decreases. Hence, the simple SOFC voltage given by (13) is higher than that of the detailed SOFC model at the nominal steady state. Fig. 10 shows a comparison of power production of the two models during the simulation. Since the voltage of the simple SOFC model is higher than that of the detailed model and the current is the same in both models, the power produced by the simple SOFC model is higher.

5.1.2. Two-volume SOFC model

Fig. 8 shows the comparison of the mean temperatures of the two SOFC models. Now, the simple SOFC is represented by aggregation of two volumes. The simple SOFC solid mean temperature is given by the average of the temperatures of the two volumes. The difference between the two mean temperatures at the nominal steady state is reduced to 51 K as supposed to 120 K. The dynamics of the two-volume model is similar to that of the dynamics of the one volume model for all the disturbances. Figs. 9 and 10 show the comparison of the voltages and powers of the two models, for the two-volume model the average voltage is plotted. There is a small voltage difference of 0.1 V between the two volumes and this is caused by the somewhat crude approximate distribution of currents between the two volumes. The two-volume model shown here can be taken as a basis to develop a multi-volume model to capture the distributed nature of the variables.

6. Hybrid system control and simulation

At first, the integrated open-loop system with double shaft configuration is simulated with a set of nominal, realistic parameters resulting in a nominal state partially shown in Table 6. As may be expected, there is a need to design a control system to compensate for load disturbances [19].

As the main source of the power in the hybrid system is the fuel flow, fuel flow must be controlled to match the power demand in case of load changes. Since it is not always possible to know the load in advance, any load change is treated as a disturbance to the controller. As the bus bar voltage is fixed when there is a load change, the current and the FU in SOFC vary. The FU cannot be varied too much since it may cause uneven temperature and voltage distributions inside the cell [14]. Hence, FU is taken as a controlled variable, where it is assumed that FU can be calculated from the measurements available.

A load change can affect the SOFC temperature to change beyond the material constraints [1,14]. Hence, the SOFC temperature should be controlled during the load changes. As there is no other free-manipulated variable

Table 6
Nominal state of the system

Variable	Value
SOFC current	250 A
Methane flow rate	0.007 kg/s
SOFC temperature	1350 K
SOFC cell voltage	0.657 V
SOFC stack power	191 kW
Generator power	87 kW
Air mass flow rate	0.445 kg/s
AU	0.23
FU	0.85
Recycle ratio	0.54
Reforming degree	0.38
Steam/methane ratio	2
I_t	1248 A
V_t	222 V
Induction motor slip	0.1

available for this purpose, a slight change must be made in the process design. After analyzing three different possible choices for an extra manipulated variable, air blow off at compressor outlet is found to be superior in terms of control authority, compared to air bypass across the heat exchanger and additional fuel to the combustion chamber. The non-linear system is linearized at its nominal state given in Table 6, and decentralized PI controllers are tuned according to the rules given in [21]. Further, RGA analysis [22] substantiates the choice of control structure. The proposed control structure is shown in Fig. 11. The PI controllers are then implemented on the non-linear system.

To evaluate the proposed control structure, the following simulation scenario is used. The system is simulated at the nominal state for 1 s. After 5 s, the following disturbances are applied in a ramp of 5 s: the mechanical load on the induction motor (P_m) is decreased to 10%, R is increased by 5 times, I_{IK} is decreased to 10% and P_{PK} is decreased to 10% which constitutes 40% load decrease on the system and the system is simulated at steady state until 20 s. After 20 s, the P_m is increased to 50% in a step. The total load change, FU and SOFC solid temperature profiles during the simulation are shown in Fig. 12. The plant inputs, i.e. fuel flow and air blow-off during the simulation are shown in Fig. 13.

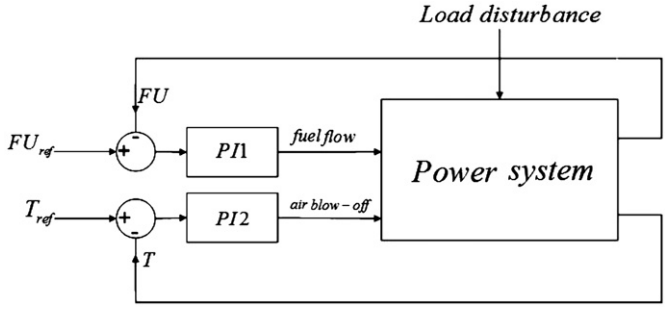

Fig. 11. Control structure.

6.1. Discussion

When there is a load decrease, correspondingly the current and amount of fuel utilized in the SOFC are decreased, which decrease the FU. To maintain FU constant at 0.85, the fuel flow rate is decreased as shown in Fig. 13. When the current decreases in the SOFC, the electrochemical reactions rate is decreased which decreases the SOFC temperature. To maintain the SOFC temperature at a constant value the air mass flow rate through the SOFC should decrease meaning that the air blow-off rate must increase as shown in Fig. 13. At the nominal state a small non-zero air blow-off rate is chosen to be able to control the SOFC temperature for any small increase in the load at the nominal value. For the 40% load change, the air blow-off rate constitutes about 18% of the total air mass flow rate which may cause a decrease in system efficiency. This is because of the strict control of the SOFC temperature at the nominal value. If the SOFC temperature is chosen to vary within some bounds around the nominal value, the air blow-off utilization can be optimized to a higher system efficiency. However, from the control point of view the proposed control structure gives satisfactory results as seen from Figs. 12 and 13. In Fig. 12, the SOFC solid temperature profile is shown which is maintained almost constant. Here it is to be noted that we wish to control the SOFC solid temperature, but not the gas temperature, hence the rapid temperature changes are not modeled as thermal inertia of gases are neglected.

It is clear that the control design must be regarded as preliminary, as there are several effects that are not accounted for, e.g. surge in the compressor and constraints on turbine inlet temperature (TIT).

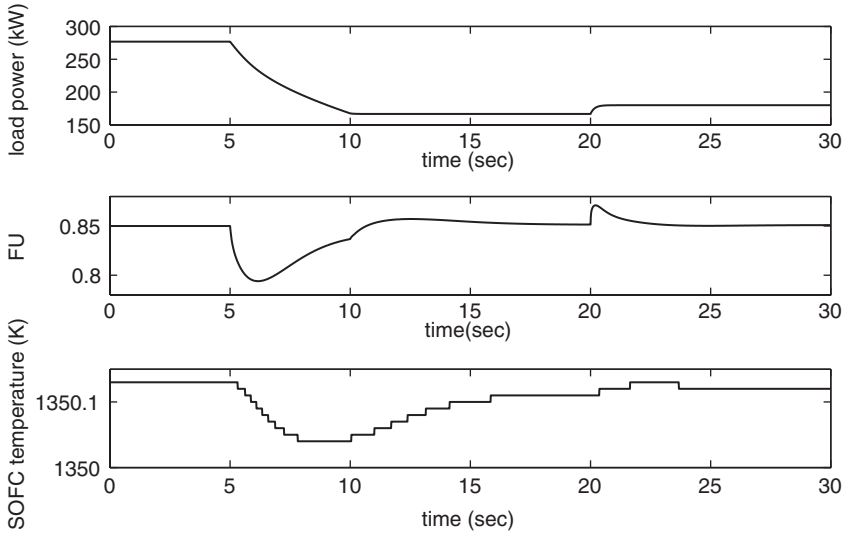

Fig. 12. Load change, FU, and SOFC temperature during simulation.

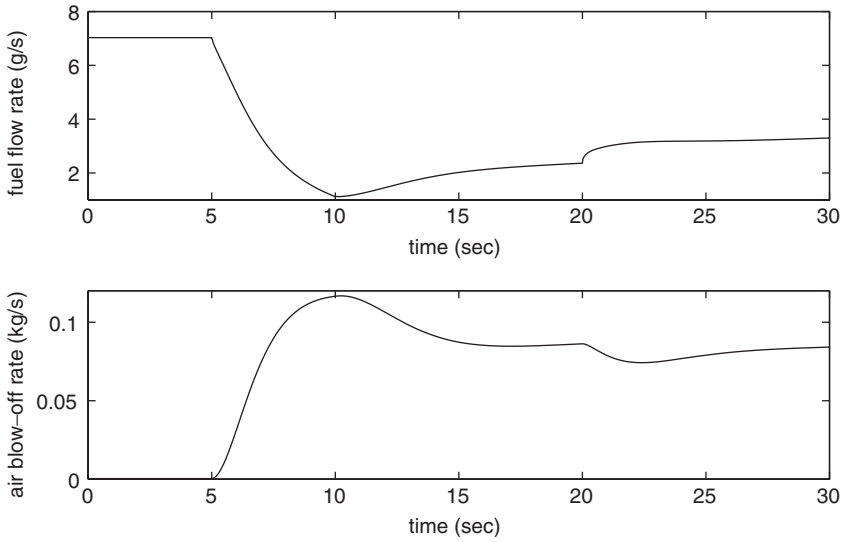

Fig. 13. Plant inputs during simulation.

7. Conclusions and further work

From the SOFC model evaluation simulation results, it is quite clear that even though there is some steady-state offset, important variables of the simple and the detailed models show similar dynamic behavior during the simulations. It can therefore be concluded that the simple model is able to capture the overall dynamics of the SOFC. This model will hence be used for further studies on control and operability of the hybrid system, i.e. an SOFC integrated in a GT cycle. If the one volume model is too crude, it is possible to aggregate a number of volumes. The results herein however indicate that a one volume model may suffice in many cases.

A model of the complete power system where a SOFC-GT hybrid system is connected to a grid with connected load is developed to include the interactions between the grid and the hybrid system. A control structure with PI controllers shows that satisfactory results can be obtained, but the main disadvantage is that the system efficiency will be reduced with the use of blow-off to control the SOFC temperature during part-load operation.

Future work will focus on optimizing the control design to reduce the air-blow-off utilization to control the SOFC temperature to increase the system efficiency at part load operation, anti-surge and TIT constraints. While the present paper focussed on control design for a two-shaft GT design, a *single-shaft* GT design which poses further challenges for a control design will also be investigated. A single-shaft GT offers the possibility of avoiding air blow-off by controlling shaft speed directly.

Notation

a_{ij}	stoichiometric matrix
A	SOFC surface area
A_{k_i}, $A_{K^{ads}}$	pre-exp. factors for k_i
C^s	solid heat capacity
DEN	denominator
E	activation energy
E^o	EMF at standard temperature and pressure
E^{OCV}	open circuit voltage
F	Faraday's constant
I	current
k_2, k_3, k_4	rate coefficients for reforming reactions
k_{an}, k_{ca}	choked flow constants
K_j	equilibrium constant for reaction j
K_i^{ads}	adsorption constant for component i
$\dot{m}$	mass flow rate
n_{rx}	number of reactions
N	number of moles
p	pressure
P	power
r_j	reaction rate of reaction j
R	universal gas constant
T	temperature
V_{an}, V_{ca}	volumes
V	voltage
$\Delta\overline{h}$	molar specific enthalpy
$\Delta\overline{h}^{rx}$	molar specific enthalpy change of reaction
$\Delta\overline{h}^{ads}$	enthalpy change of adsorption
δ	shaping factor

Subscripts and superscripts

i	chemical component
j	reaction
an	anode
ca	cathode
in	inlet
out	outlet
rad	radiation
$cond$	conduction

Acknowledgments

Financial support from The Gas Technology Center, NTNU-SINTEF and NFR is acknowledged. The second author acknowledges support from the NFR BIGCO2 project.

References

[1] Larminie J, Dicks A. Fuel cell systems explained. England: Wiley; 2003.
[2] Jensen D, Dijkstra JW. CO_2 capture in SOFC-GT systems. In: Proceedings of second annual conference on carbon sequestration, May 2003.
[3] Magistri L, Trasino F, Costamagna P. Transient analysis of a solid oxide fuel cell hybrids part A: fuel cell models. In: Proceedings of ASME Turbo Expo; 2004.
[4] Chan SH, Ho HK, Tian Y. Multi-level modeling of SOFC-gas turbine hybrid system. Int J Hydrogen Energy 2003;28(8):889–900.
[5] Pålsson J, Selimovic A, Sjunnesson L. Combined solid oxide fuel cell and gas turbine systems for efficient power and heat generation. J Power Sour 2000;86:442–8.
[6] Thorud B, Stiller C, Weydahl T, Bolland O, Karoliussen H. Part-load and load change simulation of tubular SOFC systems. In: Proceedings of fuel cell forum, Lucerne, 28 June–2 July, 2004.
[7] Hatziadoniu CJ, Lobo AA, Pourboghart F, Daneshdoost M. A simplified dynamic model of grid-connected fuel-cell generators. IEEE Trans Power Delivery 2002;17(2):467–73.
[8] Xu J, Froment GF. Methane steam reforming, methanation and water–gas shift: I. Intrinsic kinetics. AIChE J 1989;35(1):88–96.
[9] Thomas P. Simulation of industrial processes for control engineers. Wobourn, MA, USA: Butterworth-Heinemann; 1999.
[10] Lukas MD, Lee KY, Ghezel-Ayagh H. An explicit dynamic model for direct reforming carbonate fuel cell stack. IEEE Trans Energy Conver 2001;16(3).
[11] Incropera FP, De Witt DP. Fundamentals of heat and mass transfer. USA: Wiley; 2002.
[12] Stiller C, Thorud B, Seljebø S, Mathisen Ø, Karoliussen H, Bolland O. Finite-volume modeling and hybrid-cycle performance of planar and tubular solid oxide fuel cells. J Power Sour 2005;141:227–40.
[13] Campanari S. Thermodynamic model and parametric analysis of a tubular SOFC module. J Power Sour 2004;92:26–34.
[14] Stiller C, Thorud B, Bolland O, Kandepu R, Imsland L. Control strategy for a solid oxide fuel cell and gas turbine hybrid system. J Power Sour 2006;158:303–15.
[15] Warnes LAA. Electronic and electrical engineering. London: Macmillan; 1994.
[16] Navarro IR. Dynamic power system load—estimation of parameters from operational data. Lund: Media-Tryck; 2005.
[17] Hill DJ. Nonlinear dynamic load models with recovery for voltage stability studies. IEEE Trans Power Syst 1993;8(1):166–76.
[18] gPROMS (2004). gPROMS introductory user guide. Process Systems Enterprise Ltd., 2004.
[19] Stiller C, Thorud B, Bolland O. Safe dynamic operation of a simple SOFC/GT hybrid cycle. In: Proceedings of ASME Turbo Expo; 2005.
[20] Thorud B. Dynamic modelling and characterisation of a solid oxide fuel cell integrated in a gas turbine cycle. PhD thesis, Norwegian University of Science and Technology.
[21] Skogestad S. Simple analytic rules for model reduction and PID controller tuning. J Process Control 2003;13(4):291–309.
[22] Skogestad S, Postlethwaite I. Multivariable feedback control: analysis and design. USA: Wiley; 1996.
[23] Padulles J, Ault GW, McDonald JR. An integrated SOFC dynamic model power systems simulation. J Power Sour 2000;86(1): 495–500.